

Waraporn Klinbun
Rattanakosin College for Sustainable Energy
and Environment (RCSEE),
Rajamangala University
of Technology Rattanakosin,
96 moo 3, Puthamonthon Sai 5,
Salaya, Puthamonthon Nakhon Pathom 73170,
Thailand

Phadungsak Rattanadecho
Research Center of Microwave Utilization
in Engineering (R.C.M.E.),
Department of Mechanical Engineering,
Faculty of Engineering,
Thammasat University (Rangsit Campus),
99 moo 18 Klong Luang,
Pathumthani 12120,
Thailand
e-mail: ratphadu@engr.tu.ac.th

Numerical Model of Microwave Driven Convection in Multilayer Porous Packed Bed Using a Rectangular Waveguide

The present work studies numerically the heating of multilayer porous packed bed which is subjected to the microwave radiation with a rectangular waveguide. The multilayer porous packed bed consists of the layers of fine and coarse beds. The simulations of electromagnetic field are described by solving Maxwell's equations with the finite difference time domain (FDTD) method. The flow fields and the temperature profiles are determined by the solutions of the Brinkman–Forchheimer extended Darcy model, energy, and Maxwell's equations. The study aims to understand of the influences of layered configuration, layered thickness, and operating frequency on the transport processes in a multilayer porous packed bed. The results show that all parameters have significant effect on the distributions of electromagnetic field inside a waveguide, temperature profiles, and velocity fields within the multilayer porous packed bed. [DOI: 10.1115/1.4005254]

Keywords: microwave radiation, multilayer porous packed bed, rectangular waveguide, Brinkman–Forchheimer extended Darcy model, Maxwell's equation

1 Introduction

Microwave heating has become an attractive alternative heating method because the radiation can penetrate the surface and produce volumetric heat generation inside the materials, thus leading to high energy efficiency and short process time. The microwave technology is utilized in many applications, such as the domestic microwave oven, food drying, freeze drying, pasteurization, sterilization, ceramic processing, curing of rubber, changing in chemical reaction, etc. The studies of heating process in materials due to microwave energy have been investigated both experimentally [1–5] and theoretically using analytical [6–13]. Because of the complexity of the microwave heating process, numerical modeling has been widely used to study phenomena during the microwave heating. Most previous works predicted the distributions of electromagnetic fields inside cavities and waveguides from the solution of Maxwell's equations; but, other studies assumed a source term with exponential decay (Lambert's law) [14–17]. The finite difference time domain (FDTD) method has been widely used to solve Maxwell's equations [18–21]. Of many previous studies on modeling of microwave heat transfer, most were concentrated on single-layer materials. A few studies considered modeling of microwave heating of layered materials, especially a detailed study of the parametric effect on heating and flow patterns. This is because complicated of the dielectric and thermal properties in each layer as affected by the microwave field and flow field within the layered materials.

Studies in microwave heating of multilayer materials have been investigated [21–30]. Rattanadecho et al. [26] investigated microwave heating of a multilayered material in a rectangular waveguide by numerical and experimental means. Their work demonstrated the effect of antireflection layer thickness on the heating process. The results showed that absorption and distribution of temperatures within the sample microwave energy were enhanced when a layer of lower dielectric material was attached in front of the sample. In addition, Rattanadecho [27] studied both

theoretically and experimentally thawing of layered samples due to microwave energy in the oven. Variations of layered configurations and layer thickness on the degree of temperature level within the layered sample and thawing rate were shown. Recent analytical work heat and mass transfer in multilayer samples subjected to electric fields was presented by Chakranond and Rattanadecho [31]. They studied experimentally the influences of electrical voltage, particle sizes, and layer arrangement in the packed bed subjected to electrohydrodynamic (EHD). Their results showed that the single-layer packed bed with small glass beads had a higher removal rate of water and a higher rate of heat transfer than a single-layer packed bed with big glass beads. Moreover, a packed bed in the case of a fine-coarse multilayer gave drying rate higher than that given by a coarse-fine packed bed.

Investigations of microwave heating of multilayer materials are very complicated. Various effects, such as layered thickness, layered configuration, and operating frequency, are still not completely understood. The objectives of this study are to numerically analyze the effects of layered thickness, layered configuration, and operating frequency, on microwave heating of multilayer porous packed beds using rectangular waveguide. The analysis from this research serves as essential fundamentals to development of mathematic models of flow and heat transfer phenomena.

2 Mathematical Model

Figure 1(a) shows the model for microwave heating of the multilayer porous packed bed using a rectangular waveguide. The computational domain consists of the packed bed of glass beads filling the waveguide. The considered wave in TE₁₀ mode is applied along the z direction of the guide with inside dimensions of 109.22 mm × 54.61 mm (x × y). The TE₁₀ mode is one of the basic types of electromagnetic propagation by a rectangular waveguide. The TE (transverse electric) signifies that all electric fields are transverse to the direction of propagation and that no longitudinal electric field is present. The both ends of the waveguide are assumed to be absorbing conditions and the walls perfectly conducting. For temperature and flow fields, the computational domain is limited to the region enclosed by the container. Figure 1(b) shows the samples, called saturated porous packed

Contributed by the Heat Transfer Division of ASME for publication in the JOURNAL OF HEAT TRANSFER. Manuscript received January 5, 2011; final manuscript received September 30, 2011; published online February 15, 2012. Assoc. Editor: He-Ping Tan.

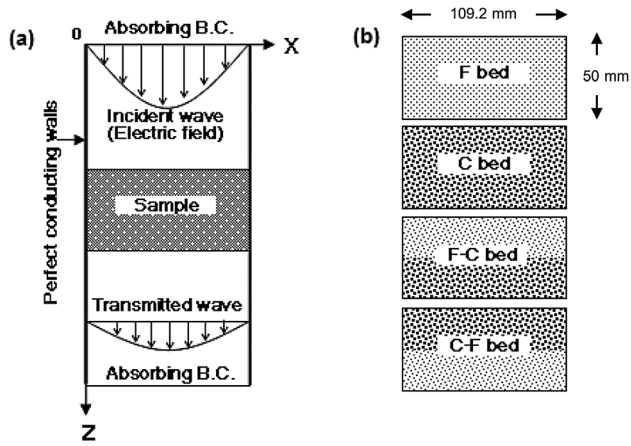


Fig. 1 Configuration model: (a) computational domain and (b) various kinds of multilayer porous packed bed (sample)

beds, which are composed of glass beads and water (water saturation(s) is 1.0). The dimensions of the packed bed are chosen to be 109.22 mm × 50 mm (x × z). The samples are prepared in two cases: a single-layer porous packed bed (fine bed with diameter of 0.15 mm (F-bed) and coarse bed with diameter of 0.40 mm (C-bed)) and the two-layer porous packed bed. In the case of two-layer porous packed bed, there are two configurations: FC-bed (fine beads with diameter of 0.15 mm on coarse beads with diameter of 0.40 mm) and CF-bed (coarse beads with diameter of 0.40 mm on fine beads with diameter of 0.15 mm).

2.1 Analysis of Electromagnetic Field. From the Fig. 1(a), this study is based on the following assumptions:

- (1) Since the electromagnetic wave in the TE₁₀ mode does not change in the direction between the broad faces, the analysis of electromagnetic field inside the guide is considered on only the x-z plane [21].
- (2) The absorption of microwave energy inside the cavity (by container and air) is neglected.
- (3) The walls of a rectangular waveguide are perfectly conducting walls.

The Maxwell's equations are solved for simulation the distribution of electromagnetic field inside the waveguide. For electromagnetic wave in TE₁₀ mode, the governing equations can be written as [21]

$$\frac{\partial E_y}{\partial z} = \mu \frac{\partial H_x}{\partial t} \quad (1)$$

$$\frac{\partial E_y}{\partial x} = -\mu \frac{\partial H_z}{\partial t} \quad (2)$$

$$-\left(\frac{\partial H_z}{\partial x} - \frac{\partial H_x}{\partial z}\right) = \sigma E_y + \varepsilon \frac{\partial E_y}{\partial t} \quad (3)$$

where permittivity or dielectric constant, ε , magnetic permeability, μ , and electric conductivity, σ , are defined by [21]

$$\varepsilon = \varepsilon_0 \varepsilon_r, \quad \mu = \mu_0 \mu_r, \quad \sigma = 2\pi f \varepsilon \tan \delta \quad (4)$$

The dielectric properties or electrical properties of a material can determine the absorption of microwave energy and consequent heating behavior of the materials in the microwave heating process. The dielectric properties are functions of moisture content and temperature, as follows [21]:

$$\varepsilon_r(s, T) = \varepsilon'_r(s, T) - j\varepsilon''_r(s, T) \quad (5)$$

where

$$\begin{aligned} [\varepsilon'_r(s, T)]^m &= \sum_{i=1}^3 v_i [\varepsilon'_{ri}(T)]^m = \phi s [\varepsilon'_{ri}(T)]^m \\ &+ \phi(1-s) [\varepsilon'_{ra}]^m + (1-\phi) [\varepsilon'_{rp}]^m \end{aligned} \quad (6)$$

$$\begin{aligned} [\varepsilon''_r(s, T)]^m &= \sum_{i=1}^3 v_i [\varepsilon''_{ri}(T)]^m = \phi s [\varepsilon''_{ri}(T)]^m \\ &+ \phi(1-s) [\varepsilon''_{ra}]^m + (1-\phi) [\varepsilon''_{rp}]^m \end{aligned} \quad (7)$$

The parameter m is varied over the range 0–1, as suggested by Wang and Schmutge [32]. For this study, a value of $m = 0.33$ was used because this value made the computational dielectric properties close to the dielectric properties from measurements.

The loss tangent coefficient $\tan \delta$ can be expressed as [21]

$$\tan \delta = \frac{\varepsilon''_r(s, T)}{\varepsilon'_r(s, T)} \quad (8)$$

2.1.1 Boundary and Initial Conditions

- (1) Perfect conduction conditions are utilized at the inner wall of the waveguide. Therefore, normal components of the magnetic field and tangential components of the electric field vanish at these walls

$$H_n = 0, \quad E_t = 0 \quad (9)$$

where subscripts t, n denote the components of tangential and normal directions, respectively.

- (2) The first order absorbing conditions by Mur [33] are used at both ends of the waveguide

$$\frac{\partial E_y}{\partial t} = \pm v \frac{\partial E_y}{\partial z} \quad (10)$$

where \pm are represented forward and backward directions and v denotes the phase velocity of the propagation wave.

- (3) The input microwave sources are simulated by these equations [21]

$$E_y = E_{y\text{in}} \sin\left(\frac{\pi x}{L_x}\right) \sin(2\pi ft) \quad (11)$$

$$H_x = \frac{E_{y\text{in}}}{Z_H} \sin\left(\frac{\pi x}{L_x}\right) \sin(2\pi ft) \quad (12)$$

where f is the frequency of microwave, L_x is the width of a rectangular waveguide, Z_H is the wave impedance, and $E_{y\text{in}}$ is the input value of the electric field intensity. By applying the Poynting theorem, the input value of the electric field intensity is evaluated using the microwave power input as

$$E_{y\text{in}} = \sqrt{\frac{4Z_H P_{\text{in}}}{A}} \quad (13)$$

where P_{in} is the microwave power input and A is the area of the incident plane.

- (4) The continuity conditions at the interface between different materials are given by

$$E_t = E'_t, \quad H_t = H'_t \quad (14)$$

$$D_n = D'_n, \quad B_n = B'_n \quad (15)$$

- (5) At $t = 0$ all components of E, H are zero.

2.2 Analysis of Flow Field and Heat Transfer. The schematic configuration of the heat and flow problem is showed in Fig. 1(b). The width and total depth of all samples are 109.22 mm and 50 mm, respectively. To reduce complexity of the problem, several assumptions have been offered into the flow and energy equations.

- (1) The effect of the phase change can be neglected.
- (2) The Boussinesq approximation takes into account of the effect of density variation on the buoyancy force.
- (3) The thermophysical properties of the sample are taken to be constant.
- (4) The solid particle is spherical, uniform shape, and incompressible.
- (5) Local thermodynamic equilibrium is assumed.

Continuity equation

$$\frac{\partial u}{\partial x} + \frac{\partial w}{\partial z} = 0 \quad (16)$$

Momentum equations

$$\frac{1}{\phi} \left(\frac{\partial u}{\partial t} \right) + \frac{1}{\phi^2} \left(u \frac{\partial u}{\partial x} + w \frac{\partial u}{\partial z} \right) = -\frac{1}{\rho_f} \left(\frac{\partial p}{\partial x} \right) + \nu \left(\frac{\partial^2 u}{\partial x^2} + \frac{\partial^2 u}{\partial z^2} \right) - \left(\frac{\nu u}{\kappa} - F(u^2 + w^2)^{1/2} u \right) \quad (17)$$

$$\frac{1}{\phi} \left(\frac{\partial w}{\partial t} \right) + \frac{1}{\phi^2} \left(u \frac{\partial w}{\partial x} + w \frac{\partial w}{\partial z} \right) = -\frac{1}{\rho_f} \left(\frac{\partial p}{\partial z} \right) + \nu \left(\frac{\partial^2 w}{\partial x^2} + \frac{\partial^2 w}{\partial z^2} \right) - \left(\frac{\nu w}{\kappa} - F(u^2 + w^2)^{1/2} w + g\beta(T - T_\infty) \right) \quad (18)$$

Energy equation

$$(\rho C_p)_{\text{eff}} \frac{\partial T}{\partial t} + (\rho C_p)_f \left(u \frac{\partial T}{\partial x} + w \frac{\partial T}{\partial z} \right) = k_{\text{eff}} \left(\frac{\partial^2 T}{\partial x^2} + \frac{\partial^2 T}{\partial z^2} \right) + Q_{\text{eff}} \quad (19)$$

where

$$(\rho C_p)_{\text{eff}} = (1 - \phi)(\rho C_p)_s + \phi(\rho C_p)_f \quad (20)$$

$$k_{\text{eff}} = (1 - \phi)k_s + \phi k_f \quad (21)$$

$$Q_{\text{eff}} = (1 - \phi)Q_s + \phi Q_f \quad (22)$$

are the overall heat capacity per unit volume, overall thermal conductivity, and overall heat generation per unit volume of the porous packed bed, respectively.

The microwave power absorbed term (Q), is a function of the electric field and dielectric properties [21].

$$Q = 2\pi f \cdot \epsilon_0 \cdot \epsilon_r' (\tan \delta) E_y^2 \quad (23)$$

The permeability κ and geometric function F in Eqs. (17) and (18) are as followed [35–37]:

$$\kappa = \frac{\phi^3 d_p^2}{175(1 - \phi)^2} \quad (24)$$

$$F = \frac{1.75(1 - \phi)}{d_p \phi^3} \quad (25)$$

The porosity near the impermeable boundaries is assumed to vary exponentially with distance along the wall, this work proposed the variation of porosity within three confined walls of the bed: a bottom wall and two lateral walls. The expression that considers the variation of porosity in two directions in the x-z plane is given by

$$\phi = \phi_\infty \left[1 + a_1 \left\{ \exp\left(\frac{-a_2 x}{d_p}\right) + \exp\left(\frac{-a_2(W-x)}{d_p}\right) + \exp\left(\frac{-a_2 z}{d_p}\right) \right\} \right] \quad (26)$$

where d_p is the diameter of glass bead, ϕ_∞ is the free stream porosity, a_1, a_2 are empirical constants, and W is the width of the packed bed. The dependencies of a_1 and a_2 to the ratio of the bed to bead diameter is small [37]. Vafai [37] suggested 0.98 and 1.0 for the values of a_1 and a_2 .

2.2.1 Boundary and Initial Conditions. Figure 1(b) shows that no slip boundary conditions are applied at all solid walls and the walls are insulated except for the upper surface which can exchange with an ambient air.

- (1) Heat is lost from the surface of the porous packed bed due to natural convection

$$-k \frac{\partial T}{\partial z} = h_c(T - T_\infty) \quad (27)$$

- (2) At the upper surface, the velocity in the normal direction (w) and the shear stress in the horizontal direction are assumed to be zero. Complete the analysis of fluid flow, the influence of Marangoni flow is applied

$$\eta \frac{\partial u}{\partial z} = -\frac{d\xi}{dT} \frac{\partial T}{\partial x} \quad (28)$$

where η is dynamic viscosity and ξ is surface tension.

- (3) The interface boundary conditions between layer 1st and layer 2nd are given by

$$k_1 \frac{\partial T_1}{\partial z} = k_2 \frac{\partial T_2}{\partial z}, \quad T_1 = T_2 \quad (29)$$

$$\eta_1 \frac{\partial u_1}{\partial z} = \eta_2 \frac{\partial u_2}{\partial z}, \quad u_1 = u_2 \quad (30)$$

- (4) The initial temperature of the porous packed bed and air inside the rectangular waveguide are constant at 28 °C.

3 Numerical Solution

The Maxwell's equations (Eqs. (1)–(3)) are solved using the FDTD method with boundary conditions given by Eqs. (9)–(15). The electric field components (E) and the magnetic field components (H) are discretized by a central difference method (second-order accurate) in both spatial and time domain [34]. The equations are solved in a leap-frog manner; the electric field is solved at a given instant in time, then the magnetic field is solved at the next time, and the process is repeated over and over again. To ensure stability of the time-stepping algorithm, Δt is chosen to satisfy the courant stability condition

$$\Delta t \leq \frac{\sqrt{(\Delta x)^2 + (\Delta z)^2}}{c} \quad (31)$$

And the spatial resolution of each cell is defined as in

$$\Delta x, \quad \Delta z \leq \frac{\lambda_g}{10\sqrt{\epsilon_r}} \quad (32)$$

In this work, a time step of $\Delta t = 2 \times 10^{-12}$ s is used to solve the Maxwell's equations. The grid sizes are $\Delta x = 1.0922$ mm and $\Delta z = 1.0$ mm.

The fluid flow and heat transport within the porous packed bed are expressed as Eqs. (16)–(19). These equations are coupled to Maxwell's equations by Eq. (23). Equations (16)–(19) are solved numerically by using a cell-centered, finite control volume along with the SIMPLE algorithm developed by Patankar [38]. The time step is 0.01 s. The reason to use this method is its advantage in flux conservation that avoids generation of parasitic sources. The basic strategy of the finite control volume discretization method is

to divide the calculated domain into a number of control volumes and then integrate the conservation equations over this control volume over an interval of time $[t, t + \Delta t]$. At the boundaries of the calculated domain, the conservation equations are discretized by integrating over half the control volume and taking into account the boundary conditions. At the corners of the calculated domain, we used a quarter of control volume. The fully implicit time-discretization finite difference scheme is used to arrive at the solution in time. Time step iterations are continued until the relative error is less than 10^{-6} (error $\leq 10^{-6}$).

4 Results and Discussion

4.1 Validation. The simulation results have been validated against the results obtained by Cha-um et al. [4]. Some of the computational data for electromagnetic field and thermophysical properties are given in Table 1. Figures 2(a) and 2(b) show the comparison for the temperature distributions within the single-layer porous packed bed (F-bed) between the predicted and previous results [4] as a function of width (x) at various depths and various times, respectively. The field variables for the comparison were chosen as: $P = 300$ W, $f = 2.45$ GHz, $d_p = 0.15$ mm. From the figures, one sees that the predicted temperature distribution and experimental data [4] are in good agreement and the differences lie within 3°C . It was found that the previous experimental study [4] considered only the single-layer porous packed bed. However, in practical applications of microwave heating, most samples are multilayer porous materials. The structure has a significant effect on temperature and velocity profiles.

4.2 Parametric Study. In this study, the influences of three parameters, such as the layered configuration (the single and multilayer porous packed bed), the layered thickness (1F3C, 2F2C, and 3F1C), and the operating frequency (1.5, 2.45, and 5.8 GHz) have been investigated. From parametric studies we observe the effects of each of these factors, separately, and analyze their contributions in determining the electric field distributions and temperature and velocity profiles.

Thus, the following cases have been considered:

- (1) The single and multilayer porous packed bed with fixed power input ($P = 500$ W), operating frequency ($f = 2.45$ GHz), and the layered thickness (2F2C and 2C2F).
- (2) The multilayer porous packed bed with fixed power input ($P = 500$ W), operating frequency ($f = 2.45$ GHz), and the layered configuration (FC-bed).
- (3) The multilayer porous packed bed with fixed layered configuration (FC-bed), the layered thickness (2F2C), and power input ($P = 500$ W).

The distributions of electric field inside a rectangular waveguide, temperature, and flow field within the porous packed bed were shown for all cases.

4.3 Effect of Layered Configuration. In this topic, the effect of layered configuration is studied. The simulations are displayed for four different configurations, namely, F-bed,

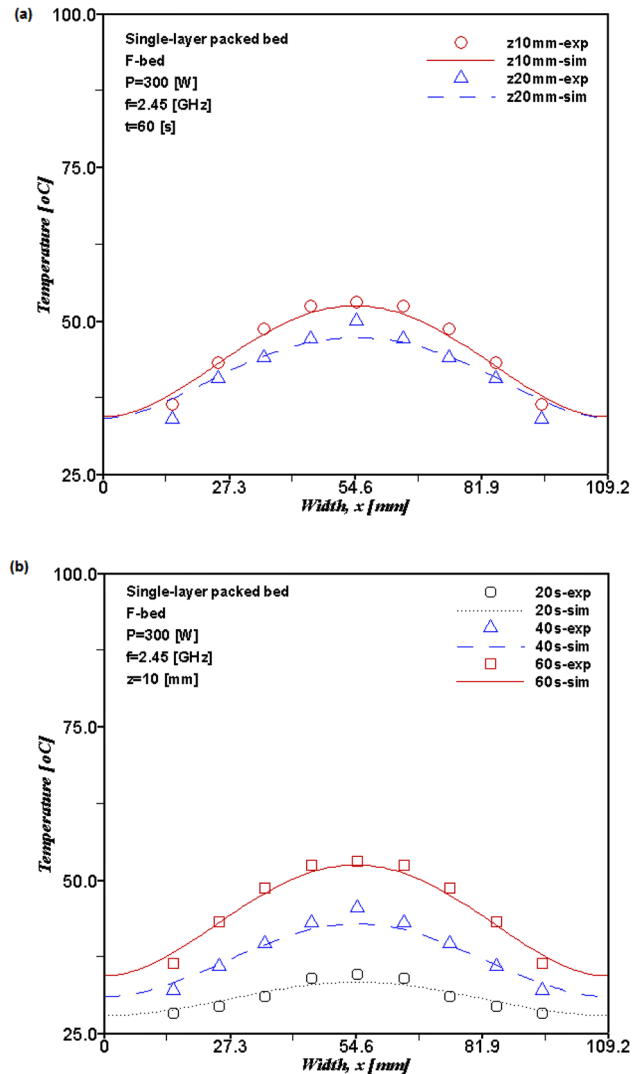


Fig. 2 Temperature distribution within single-layer porous packed bed: Comparison with experiment

C-bed, 2F2C-bed, and 2C2F-bed. The physical data are: $P = 500$ W, $f = 2.45$ GHz, and $t = 60$ s. In case of the multilayer porous packed bed, layer thickness of the fine bed is equal to the coarse bed thickness, 25.0 mm. Figure 3 shows the distribution of electric field in the TE_{10} mode along the center axis ($x = 54.61$ mm) of the rectangular waveguide at different layered configurations. As shown in the figure, the vertical axis represents the electric field intensity, E_y , which is divided by the input electric field, $E_{y\text{in}}$. Figures 3(a) and 3(b) show a standing wave with strong amplitude is formed inside the cavity and is extinguished within the sample. This is because the permittivity of air inside the cavity is lower than the permittivity of the packed bed, thus, the majority

Table 1 The dielectric and thermal properties in computations [21]

| | | |
|--|---|--------------------------------------|
| $\epsilon_0 = 8.85419 \times 10^{-12}$ (F/m) | $\mu_0 = 4\pi \times 10^{-7}$ (H/m) | |
| $\epsilon_{ra} = 1.0$ | $\epsilon_{rp} = 5.1$ | |
| $\mu_{ra} = 1.0$ | $\mu_{rp} = 1.0$ | $\mu_{rw} = 1.0$ |
| $\tan \delta_a = 0.0$ | $\tan \delta_p = 0.01$ | |
| $\rho_a = 1.205$ (kg/m ³) | $\rho_p = 2500$ (kg/m ³) | $\rho_w = 1000$ (kg/m ³) |
| $C_{pa} = 1.007$ [kJ/(kgK)] | $C_{pp} = 0.80$ [kJ/(kgK)] | $C_{pw} = 4.186$ [kJ/(kgK)] |
| $\epsilon_{rw} = 88.15 - 0.414T + (0.131 \times 10^{-2})T^2 - (0.046 \times 10^{-4})T^3$ | $\tan \delta_w = 0.323 - (9.499 \times 10^{-3})T + (1.27 \times 10^{-4})T^2 - (6.13 \times 10^{-7})T^3$ | |

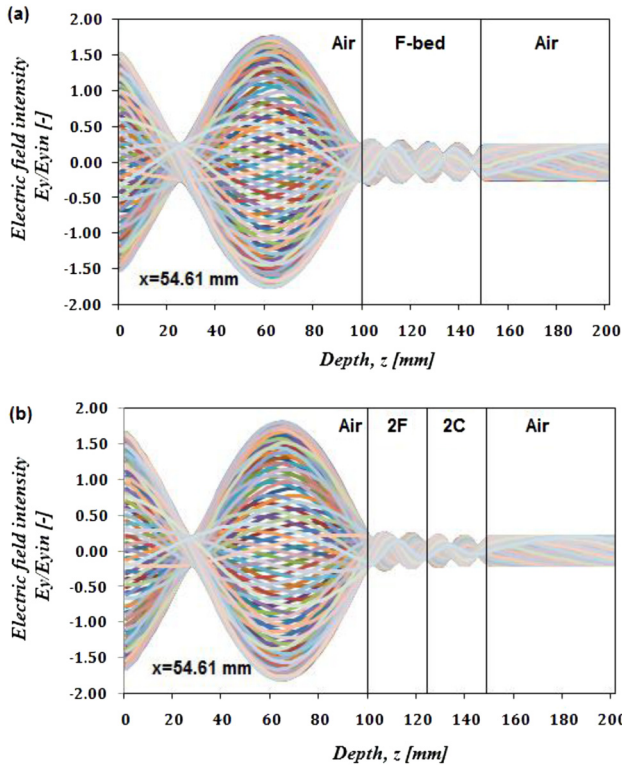


Fig. 3 Distribution of electric field inside a rectangular waveguide: Effect of layered configuration (a) in case F-bed and (b) in case 2F2C-bed

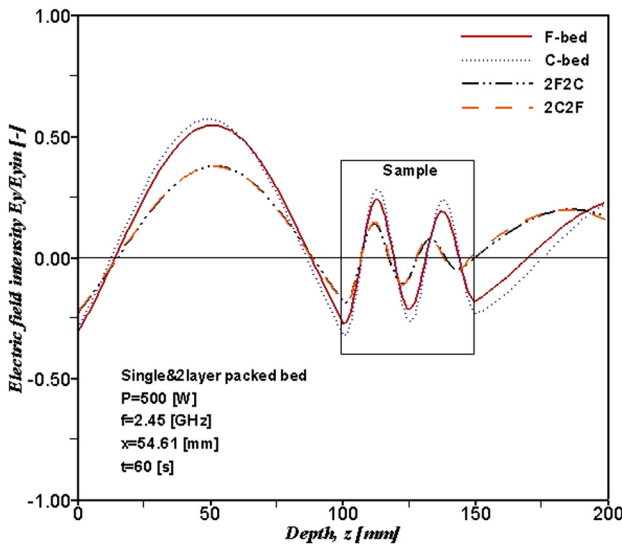


Fig. 4 Comparison of electric field distribution between single and multilayer porous packed bed

of the incident wave is reflected and resonated while the minor part is transmitted. Figure 4 shows the comparison of electric field intensity for each case along with z-axis of the waveguide. It reveals the large amplitude of electric field corresponding to the case of the single-layer porous packed bed (F, C-bed). Since the structure of the single-layer porous packed beds is uniform the electric field amplitude is higher. Considering the distribution of electric field in the case of the multilayer porous packed bed (2F2C and 2C2F), one finds a similar profile with a slight difference in magnitude.

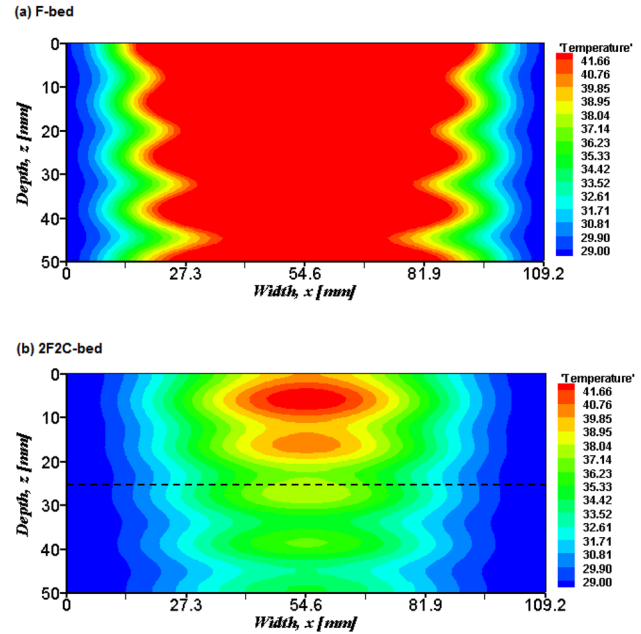


Fig. 5 Temperature distribution within porous packed bed: effect of layered configuration (a) in case F-bed and (b) in case 2F2C-bed ($P = 500$ W, $f = 2.45$ GHz, and $t = 60$ s)

Temperature profiles within the single and multilayer porous packed bed at $t = 60$ s are shown in Figs. 5(a) and 5(b), respectively. It is found that the temperature profiles show excellent agreement with the electric field distribution. Figure 5 shows that the temperature is highest at the center of the porous packed bed and distributes to the wall because standing waves are formulated within the porous packed bed. The comparison of temperature profiles between the single and multilayer porous packed bed along x and z axis are displayed in Figs. 6(a) and 6(b), respectively. Figure 6(a) shows that the temperature is highest at the center of the packed bed. This is because the intensity of electric field in the TE_{10} mode is high around the middle of the guide. Figure 6(b) shows that the highest temperature is at the surface of the porous packed bed and decreases along the depth of the packed bed due to the penetration depth of the microwave. It is interesting to observe that the temperature of the single-layer porous packed bed is higher than the temperature of the multilayer porous packed bed. This is because the incident wave can penetrate and convert to thermal energy in the uniform packed bed (single-layer) higher than that in the case nonuniform packed bed (multilayer). In case of the single-layer, the temperature of the C-bed is higher than the temperature of the F-bed due to the effect of the glass bead arrangement. The porous packed bed with small glass beads aligned quite tightly with the big glass beads results in higher reflected wave intensity from the packed bed.

Velocity fields within the single and multilayer porous packed bed at $t = 60$ s are illustrated in Fig. 7. From the figure, one sees that the layered arrangement has important effects on the velocity field, due to the permeability, κ , of the porous packed bed. The flow pattern is symmetrical between left and right sides. In case of an attaching fine bed on the coarse bed (2F2C-bed), as shown in Fig. 7(b), both layers have strong velocity fields. This causes the upper layer (F-bed) receive strong incident wave while the bottom layer (C-bed) is of high permeability. On the other hand, the attaching fine bed under the coarse bed (2C2F-bed) is illustrated in Fig. 7(c). It is shown that the velocity field in the bottom layer (F-bed) is very weak. Since the permeability of the porous packed bed with the small glass beads (F-bed) is low, many glass beads resist the flow motion of liquid in the voids. Moreover, the bottom

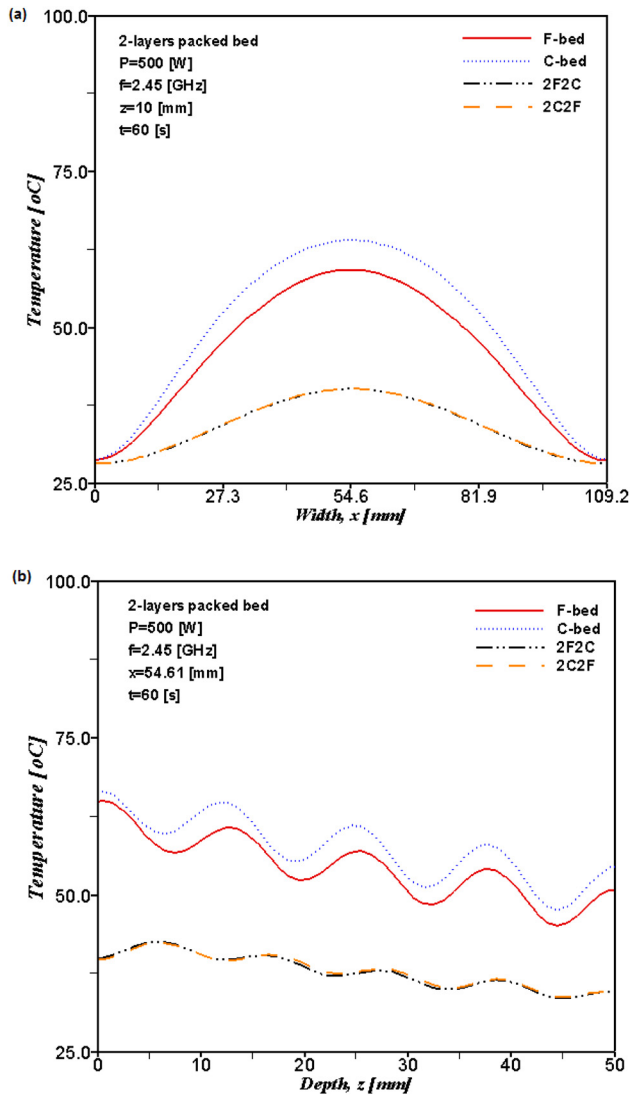


Fig. 6 Comparison of temperature profile between single and multilayer porous packed bed: (a) along x-axis and (b) along z-axis

layer has received a weakened microwave field. In addition, Fig. 7(c) indicates that with low permeability, the convective heat transfer mechanism is almost suppressed, while conduction plays an important role in heat transfer.

4.4 Effect of Layered Thickness. It is interesting to investigate the effects of changing the layered thickness because it makes the different samples have different heating and flow patterns. The simulation of electric field distributions and temperature and velocity profiles are shown for various layered thicknesses, such as 1F3C ($z_F = 12.5$ mm and $z_C = 37.5$ mm), 2F2C ($z_F = 25.0$ mm and $z_C = 25.0$ mm), and 3F1C ($z_F = 37.5$ mm and $z_C = 12.5$ mm) where the configuration of the porous packed bed is FC-bed (attaching fine bed on coarse bed). The physical data are: $P = 500$ W, $f = 2.45$ GHz, and $t = 60$ s. Figure 8 shows the comparison of electric field intensity between the different layered thicknesses along z-axis of a rectangular waveguide in the TE₁₀ mode. As seen from the figure, the amplitudes of the electric fields are high over the surface of the packed bed (left hand side) and almost extinguished within the packed bed. It is found that the distributions of electric fields are same pattern but are a little different in magnitude for each case.

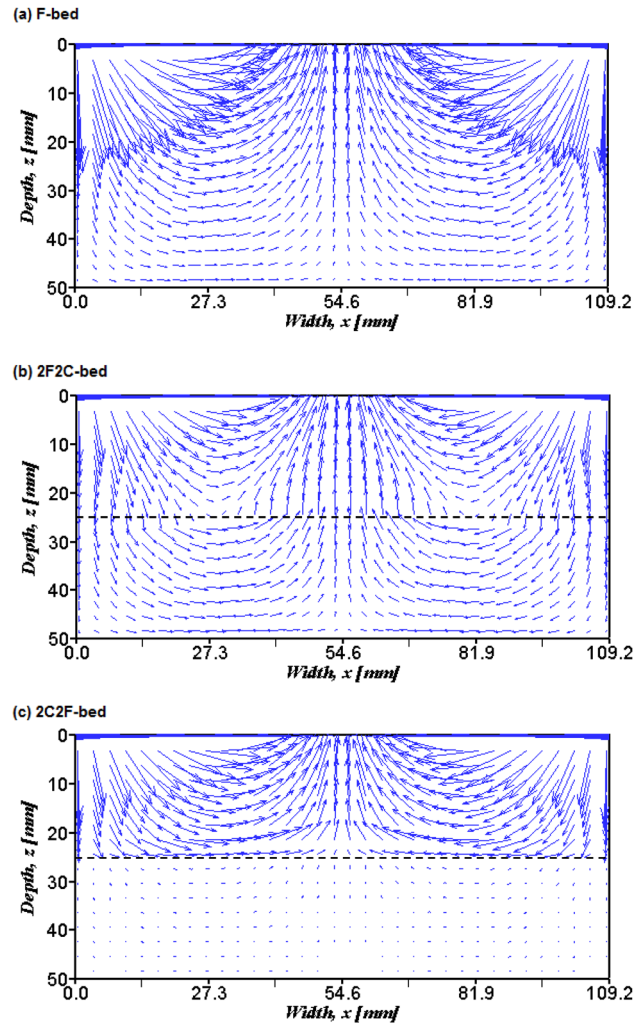


Fig. 7 Velocity field within multilayer porous packed bed: effect of layered configuration (a) in case F-bed, (b) in case 2F2C-bed, and (c) in case 2C2F-bed ($P = 500$ W, $f = 2.45$ GHz, and $t = 60$ s)

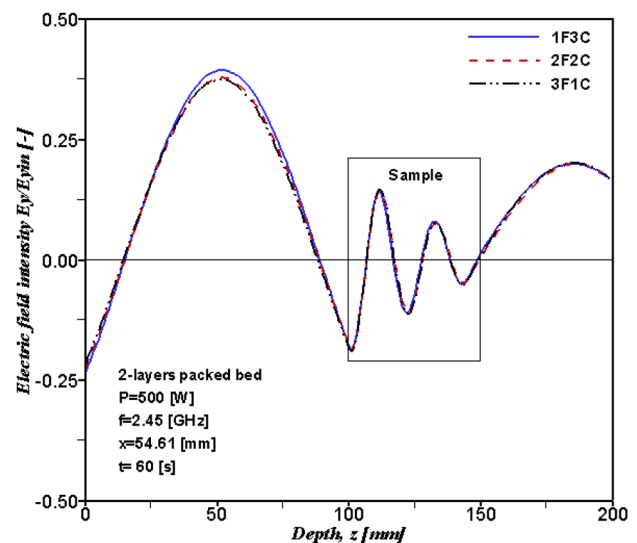


Fig. 8 Comparison of electric field distribution between different layered thicknesses

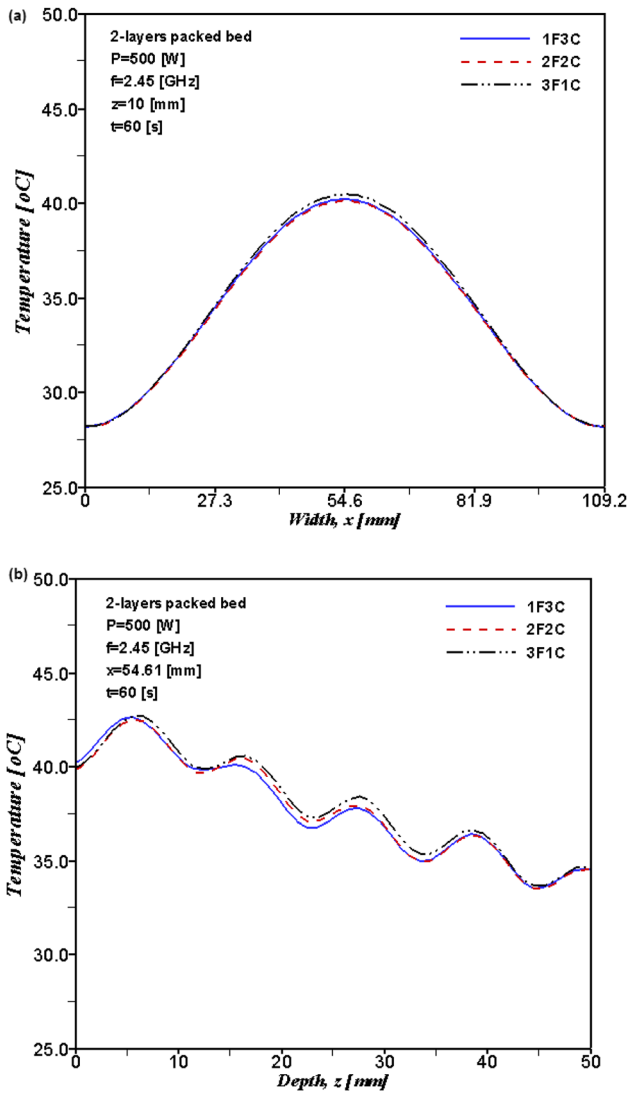


Fig. 9 Comparison of temperature profile between different layered thicknesses: (a) along x-axis and (b) along z-axis

Figures 9(a) and 9(b) illustrate temperature profiles within the multilayer porous packed bed with various layered thicknesses along the x and z axes, respectively. It is observed that the highest temperature occurs at the center and upper surface of the packed bed for the 3F1C-bed case. It indicates the effect of layered thickness on heat transfer. Figures 10(a) and 10(b) show flow fields of water in the voids at $t = 60$ s for the 1F3C and 3F1C-beds, respectively. The velocity fields of both layers clearly separate at the interface between the layers. However, the patterns are similar to each other. As already explained in the previous topic, the key factor affecting the flow of fluid in the multilayer porous packed bed is permeability, κ , of each layer.

4.5 Effect of Operating Frequency. Changes in the operating frequencies have significant effects on the electric field distribution and temperature and velocity fields. This study has three frequencies in the range of application, 1.5, 2.45, and 5.8 GHz. The physical data are: $P = 500$ W, 2F2C-bed and $t = 60$ s. Figures 11(a) and 11(b) show the electric field distribution inside a rectangular waveguide when the 2F2C packed bed is inserted in the waveguide during microwave heating with operating frequency of 1.5 and 5.8 GHz, respectively. In the case of 1.5 GHz, the penetration depth of microwave is higher than the total depth

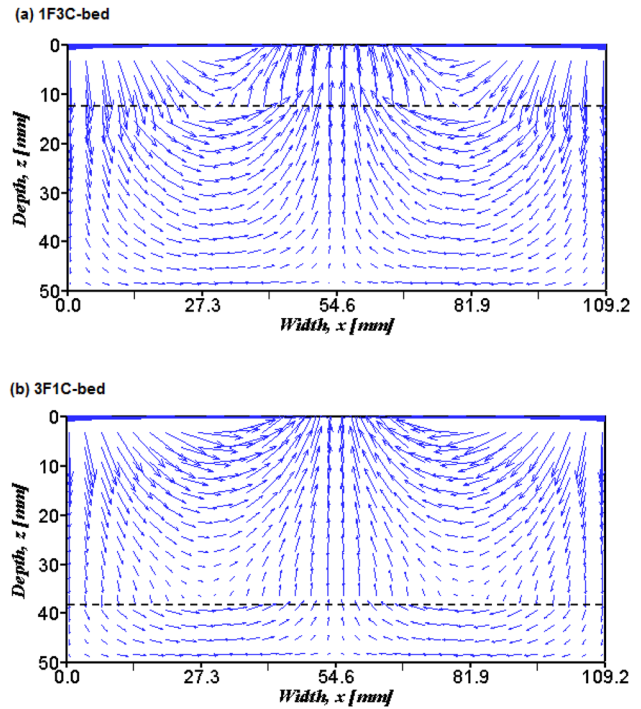


Fig. 10 Velocity field within FC-bed: Effect of layered thickness (a) in case 1F3C-bed and (b) in case 3F1C-bed ($P = 500$ W, $f = 2.45$ GHz, and $t = 60$ s)

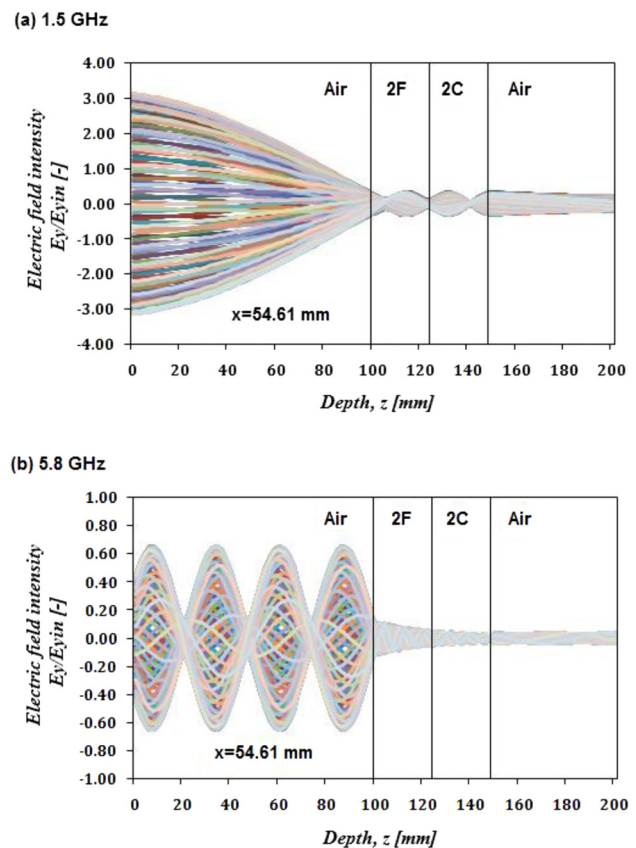


Fig. 11 Distribution of electric field inside a rectangular waveguide: effect of operating frequency (a) in case 1.5 GHz and (b) in case 5.8 GHz

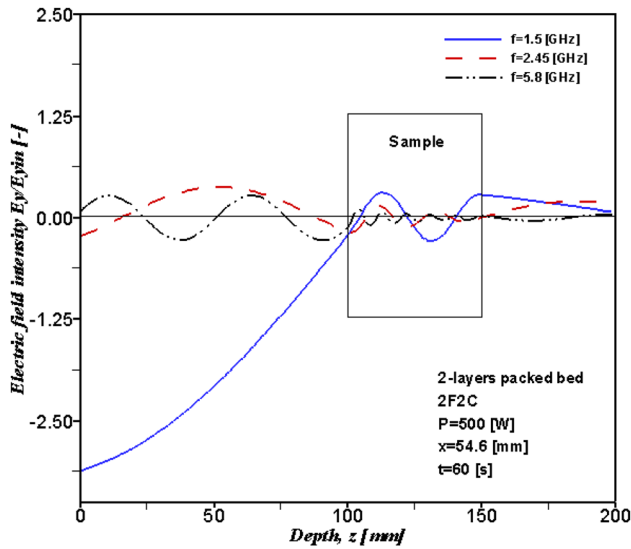


Fig. 12 Comparison of electric field distribution between different operating frequencies

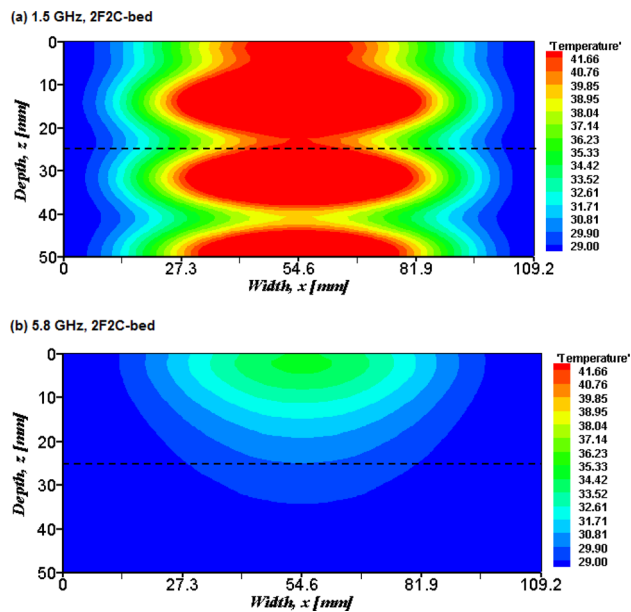


Fig. 13 Temperature distribution within 2F2C-bed: Effect of operating frequency (a) in case 1.5 GHz and (b) in case 5.8 GHz ($P = 500$ W and $t = 60$ s)

of the porous packed bed; thus, a majority of the incident wave penetrates and transmits to the packed bed (as seen in Fig. 11(a)). In contrast, in the case of 5.8 GHz, the microwave operating at a high frequency has a shorter wavelength which corresponds to smaller penetration depth compared with the depth of the porous packed bed. Therefore, the incident wave can penetrate and are absorbed only within the upper surface of the packed bed. A comparison of electric field magnitudes for various operating frequencies is illustrated in Fig. 12. The highest amplitude of the electric field corresponds to a frequency of 1.5 GHz while the frequency of 5.8 GHz as the lowest electric field amplitude.

Figures 13(a) and 13(b) display the temperature contour within the 2F2C-bed at the frequency of 1.5 and 5.8 GHz, respectively. It

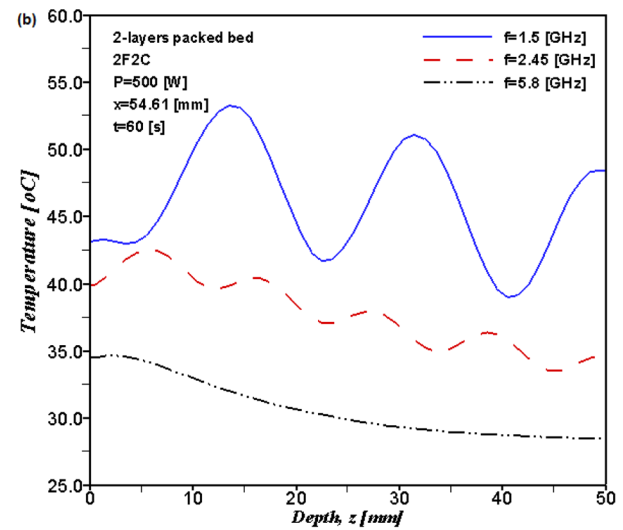
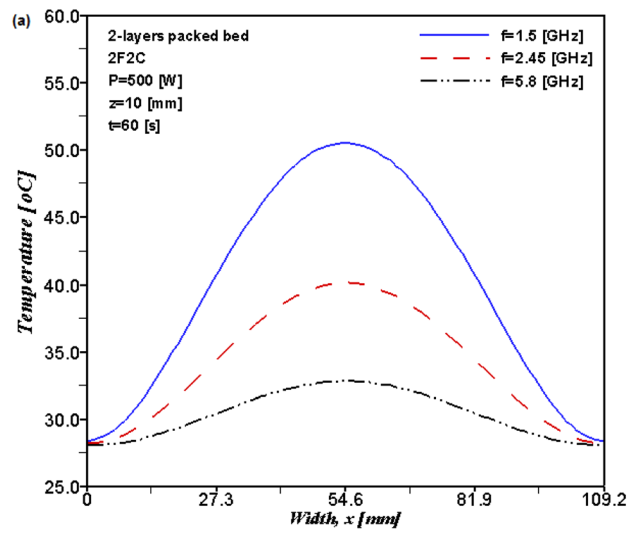


Fig. 14 Comparison of temperature profile between different operating frequencies: (a) along x-axis and (b) along z-axis

is shown that the temperature profiles display a wavy behavior corresponding to the resonance of electric field. This is because the electric field within the porous packed bed attenuates owing to energy absorption, and, thereafter, the absorbed energy is converted to thermal energy, which increases the packed bed temperature. Figures 14(a) and 14(b) show comparisons of temperature distributions within the 2F2C-bed between various microwave frequencies along x and z axis, respectively. From the figures one sees that the highest and lowest temperatures correspond to the case of frequencies at 1.5 and 5.8 GHz, respectively. Since the high frequency (5.8 GHz) leads to small penetration depth and electric field decay is faster than that of the lower frequency. Thus, the microwave power absorbed is the greatest at the surface exposed to the incident microwaves, and decays exponentially along the propagating direction with a very small wavelength, resulting in a thinner thermally stratified layer (Fig. 13(b)).

The flow fields within the 2F2C-bed at operating frequencies of 1.5 and 5.8 GHz are displayed in Figs. 15(a) and 15(b), respectively. Fluid flow fields are in the same direction but the magnitudes of velocity are clearly different. The explanation of flow behaviors was discussed in the section on the effects of layered configuration.

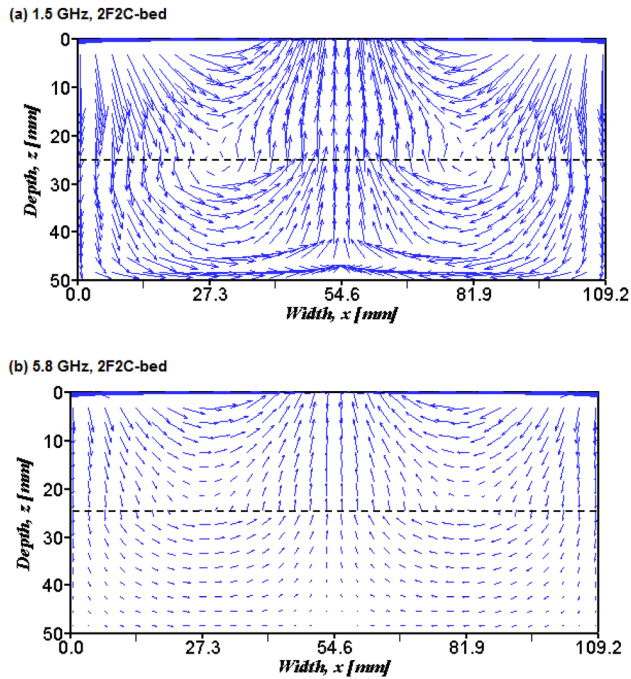


Fig. 15 Velocity field within 2F2C-bed: Effect of operating frequency (a) in case 1.5 GHz and (b) in case 5.8 GHz ($P = 500$ W and $t = 60$ s)

5 Conclusions

A numerical study is carried out to observe the effects of layered configuration, layered thickness, and operating frequency in the case of the microwave heating of the multilayer porous packed bed. The simulation results are validated with experimental data from previous work. Thus, the conclusions of this work can be summarized as following:

- (1) The modeling of heating of the multilayer porous packed bed by microwave energy with a rectangular waveguide (TE₁₀ mode) is presented and this model can use to successfully explain the heating phenomena under various conditions.
- (2) The layered configuration of the porous packed bed has significant effects on the heating pattern and velocity field.
- (3) The uniform porous packed bed with large particles corresponds to the highest temperatures.
- (4) The temperature increases with increase in the fine bed thickness.
- (5) Lower operating frequencies can generate the highest temperatures.

The next steps of this research will be to investigate more associated parameters and more details of the position of a sample inside the waveguide and to develop a three-dimensional mathematical model.

Acknowledgment

The authors gratefully acknowledge the financial support for this work provided by the Thailand Research Fund (TRF) and Higher Education Research Promotion and National Research University Project of Thailand, Office of the Higher Education Commission.

Nomenclature

- A = area (m²)
 a_1, a_2 = empirical constants
 C_p = specific heat capacity (J/(kg K))

- E = electric fields intensity (V/m)
 f = frequency of incident wave (Hz)
 F = geometric function
 g = gravitational constant (m/s²)
 h_c = local heat transfer coefficient (W/m²K)
 H = magnetic field intensity (A/m)
 k = thermal conductivity (W/mK)
 L_x = width of the rectangular waveguide (m)
 P = power (W)
 p = pressure (Pa)
 Q = local electromagnetic heat generation term (W/m³)
 s = moisture content
 T = temperature (°C)
 t = time (s)
 $\tan \delta$ = dielectric loss coefficient
 u, w = velocity component (m/s)
 W = width of packed bed (m)
 Z_H = wave impedance (Ω)
 Z_l = intrinsic impedance (Ω)

Greek Symbols

- ϕ = porosity
 α = thermal diffusivity (m²/s)
 β = coefficient of thermal expansion (1/K)
 η = dynamic viscosity (Pa/s)
 ε = permittivity (F/m)
 λ = wavelength (m)
 κ = permeability (m²)
 μ = magnetic permeability (H/m)
 v = velocity of propagation (m/s)
 ν = kinematics viscosity (m²/s)
 ρ = density (kg/m³)
 σ = electric conductivity (S/m)
 ω = angular frequency (rad/s)
 ζ = surface tension (N/m)

Subscripts

- 0 = free space
 ∞ = ambient condition
 a = air
 C = coarse bead
 eff = effective
 f = fluid
 F = fine bead
 j = layer number
 s = solid
 r = relative
 in = input
 l = liquid
 x, y, z = axis

References

- [1] Prosetya, H., and Datta, A. K., 1991, "Batch Microwave Heating of Liquids: An Experimental Study," *J. Microwave Power Electromagn. Energy*, **26**(14), pp. 215–226.
- [2] Swain, M. V. L., Russell, S. L., Clarke, R. N., and Swain, M. J., 2004, "The Development of Food Stimulants for Microwave Oven Testing," *Int. J. Food Sci. Technol.*, **39**(6), pp. 623–630.
- [3] Rattanadecho, P., Suwannapum, N., Watanasungsit, A., and Duangduen, A., 2007, "Drying of Dielectric Materials Using Microwave—Continuous Belt Furnace," *ASME J. Manuf. Sci. Eng.*, **129**(1), pp. 157–163.
- [4] Cha-um, W., Pakdee, W., and Rattanadecho, P., 2009, "Experimental Analysis of Microwave Heating of Dielectric Materials Using a Rectangular Wave Guide (MODE: TE₁₀) (Case Study: Water Layer and Saturated Porous Medium)," *Exp. Therm. Fluid Sci.*, **33**(3), pp. 472–481.
- [5] Vongpradubchai, S., and Rattanadecho, P., 2009, "The Microwave Processing of Wood Using a Continuous Microwave Belt Drier," *Chem. Eng. Process. Intensification*, **48**(5), pp. 997–1003.
- [6] Shou-Zheng, Z., and Han-Kui, C., 1988, "Power Distribution Analysis in Rectangular Microwave Heating Applicator With Stratified Load," *J. Microwave Power Electromagn. Energy*, **23**(2), pp. 139–143.

- [7] Watanabe, W., and Ohkawa, S., 1978, "Analysis of Power Density Distribution in Microwave Ovens," *J. Microwave Power Electromagn. Energy*, **13**(2), pp. 173–182.
- [8] Ayappa, K. G., Davis, H. T., Davis, E. A., and Gordan, J., 1992, "Two-Dimensional Finite Element Analysis of Microwave Heating," *AIChE J.*, **38**, pp. 1577–1592.
- [9] Datta, A., Prosetya, H., and Hu, W., 1992, "Mathematical Modeling of Batch Heating of Liquids in a Microwave Cavity," *J. Microwave Power Electromagn. Energy*, **27**, pp. 38–48.
- [10] Zhang, Q., Jackson, T. H., and Ungan, A., 2000, "Numerical Modeling of Microwave Induced Natural Convection," *Int. J. Heat Mass Transfer*, **43**, pp. 2141–2154.
- [11] Knoerzer, K., Regier, M., and Schubert, H., 2006, "Microwave Heating: A New Approach of Simulation and Validation," *Chem. Eng. Technol.*, **29**(7), pp. 796–801.
- [12] Zhu, J., Kuznetsov, A. V., and Sandeep, K. P., 2007, "Mathematical Modeling of Continuous Flow Microwave Heating of Liquids (Effects of Dielectric Properties and Design Parameters)," *Int. J. Therm. Sci.*, **46**, pp. 328–341.
- [13] Chatterjee, S., Basak, T., and Das, S. K., 2007, "Microwave Driven Convection in a Rotating Cylindrical Cavity: A Numerical Study," *J. Food Eng.*, **79**, pp. 1269–1279.
- [14] Ni, H., Datta, A. K., and Torrance, K. E., 1999, "Moisture Transport in Intensive Microwave Heating of Biomaterials: A Multiphase Porous Media Model," *Int. J. Heat Mass Transfer*, **42**(8), pp. 1501–1512.
- [15] Datta, A. K., and Ni, H., 2002, "Infrared and Hot-Air-Assisted Microwave Heating of Foods for Control of Surface Moisture," *J. Food Eng.*, **51**(4), pp. 355–364.
- [16] Campanone, L. A., and Zaritzky, N. E., 2005, "Mathematical Analysis of Microwave Heating Process," *J. Food Eng.*, **69**(3), pp. 359–368.
- [17] Curet, S., Rouaud, O., and Boillereaux, L., 2008, "Microwave Tempering and Heating in a Single-Mode Cavity: Numerical and Experimental Investigations," *Chem. Eng. Process.*, **47**, pp. 1656–1665.
- [18] Liu, F., Turner, I., and Bialkowski, M., 1994, "A Finite-Difference Time-Domain Simulation of Power Density Distribution in a Dielectric Loaded Microwave Cavity," *J. Microwave Power Electromagn. Energy*, **29**, pp. 138–147.
- [19] Zhao, H., and Turner, I. W., 1996, "An Analysis of the Finite-Difference Time-Domain Method for Modeling the Microwave Heating of Dielectric Materials Within a Three-Dimensional Cavity System," *J. Microwave Power Electromagn. Energy*, **31**, pp. 199–214.
- [20] Ma, L. H., Paul, D. L., Potheary, N., Railton, C., Bows, J., Barratt, L., et al., 1995, "Experimental Validation of a Combined Electromagnetic and Thermal FDTD Model of a Microwave-Heating Process," *IEEE Trans. Microwave Theory Tech.*, **43**(11), pp. 2565–2572.
- [21] Rattanadecho, P., Aoki, K., and Akahori, M., 2002, "Influence of Irradiation Time, Particle Sizes, and Initial Moisture Content During Microwave Drying of Multi-Layered Capillary Porous Materials," *ASME Trans. J. Heat Transfer* **124**, pp. 151–161.
- [22] Gori, F., Gentili, G., and Matini, L., 1987, "Microwave Heating of Porous Media," *ASME Trans. J. Heat Transfer* **109**, pp. 522–525.
- [23] Ayappa, K. G., Davis, H. T., Davis, E. A., and Gordan, J., 1991, "Analysis of Microwave Heating of Materials With Temperature-Dependent Properties," *AIChE J.*, **37**, pp. 313–322.
- [24] Barringer, S. A., Ayappa, K. G., Davis, E. A., Davis, H. T., and Gordan, J., 1995, "Power Absorption During Microwave Heating of Emulsions and Layered Systems," *J. Food Sci.*, **60**, pp. 1132–1136.
- [25] Rattanadecho, P., Aoki, K., and Akahori, M., 2002, "The Characteristics of Microwave Melting of Frozen Packed Beds Using a Rectangular Waveguide," *IEEE Trans. Microwave Theory Tech.*, **50**(6), pp. 1495–1502.
- [26] Rattanadecho, P., Aoki, K., and Akahori, M., 2002, "Experimental Validation of a Combined Electromagnetic and Thermal Model for a Microwave Heating of Multi-layered Materials Using a Rectangular Wave Guide," *ASME Trans. J. Heat Transfer*, **124**, pp. 992–996.
- [27] Rattanadecho, P., 2004, "Theoretical and Experimental Investigation of Microwave Thawing of Frozen Layer Using a Microwave Oven (Effects of Layered Configurations and Layer Thickness)," *Int. J. Heat Mass Transfer*, **47**, pp. 937–945.
- [28] Basak, T., and Meenakshi, A., 2006, "Influence of Ceramic Supports on Microwave Heating for Composite Dielectric Food Slabs," *AIChE J.*, **52**(6), pp. 1995–2007.
- [29] Samanta, S. K., and Basak, T., 2008, "Theoretical Analysis of Efficient Microwave Processing of Oil-Water Emulsions Attached With Various Ceramic Plates," *Food Res. Int.*, **41**, pp. 386–403.
- [30] Samanta, S. K., Basak, T., and Sengupta, B., 2008, "Theoretical Analysis on Microwave Heating of Oil-Water Emulsions Supported on Ceramic, Metallic or Composite Plates," *Int. J. Heat Mass Transfer*, **51**(25–26), pp. 6136–6156.
- [31] Chakranon, C., and Rattanadecho, P., "Analysis of Heat and Mass Transfer Enhancement in Porous Material Subjected to Electric Fields (Effects of Particle Sizes and Layer Arrangement)," *Exp. Therm. Fluid Sci.* (in press).
- [32] Wang, J., and Schmugge, T., 1980, "An Empirical Model for the Complex Dielectric Permittivity of Soil as a Function of Water Content," *IEEE Trans. Geosci. Remote Sens.*, **GE-18**(4), pp. 288–295.
- [33] Mur, G., 1981, "Absorbing Boundary Conditions for the Finite Difference Approximation of the Time Domain Electromagnetic Field Equations," *IEEE Trans. Electromagn. Compat.*, **23**, pp. 377–382.
- [34] Yee, K. S., 1966, "Numerical Solution of Initial Boundary Value Problem Involving Maxwell's Equations in Isotropic Media," *IEEE Trans. Antennas Propag.*, **14**, pp. 302–307.
- [35] Nield, D. A., and Bejan, A., 1999, *Convection in Porous Media*, 2nd ed., Springer-Verlag, Inc., New York.
- [36] Ingham, D. B., and Pop, I., 1998, *Transport Phenomena in Porous Media*, Pergamon, Oxford.
- [37] Vafai, K., 2004, *Handbook of Porous Media*, Vol. II, Marcel Dekker, New York.
- [38] Patankar, S. V., 1980, *Numerical Heat Transfer and Fluid Flow*, Hemisphere/McGraw-Hill, New York.